3.2.3 OTSK13

A. Algorithm Outline

(1) Algorithm Code: OTSK13

(2) Product Code: SST_b, QF_ST

(3) PI names: G-0068 Hiroshi Kawamura

(4) Overview of algorithm (Standard level)

The GLI Sea Surface Temperature (SST) algorithm contains the following two process: the cloud detection and the atmospheric correction. The former is a process to find clear, or no cloud-contaminated, pixels in the image. The latter is need to obtain SST of clear pixels from the brightness temperatures observed by GLI. Accurate SST retrieval depends on the success of these processes.

As for the cloud detection, the combination of the threshold tests is used to detect clouds. A pixel, which passes through all the tests, is flagged as clear. The tests need to set coefficients and thresholds; they are adjusted using the real GLI data after the launch of ADEOS-II.

As for the atmospheric correction, the Multi-Channel SST (MCSST) technique is used. The radiative transfer model and the match-up dataset are used to determine the coefficients of the MCSST equation. The methodology follows in that done in OCTS SST retrieval (Sakaida et al., 1998)

B. Theoretical Description

(1) Methodology and Logic flow

The whole of the process: The whole process is summarized in the following chart (Fig.1). As mentioned above, the GLI SST products are obtained through the cloud detection and the atmospheric correction. The detail of each process will be described later.

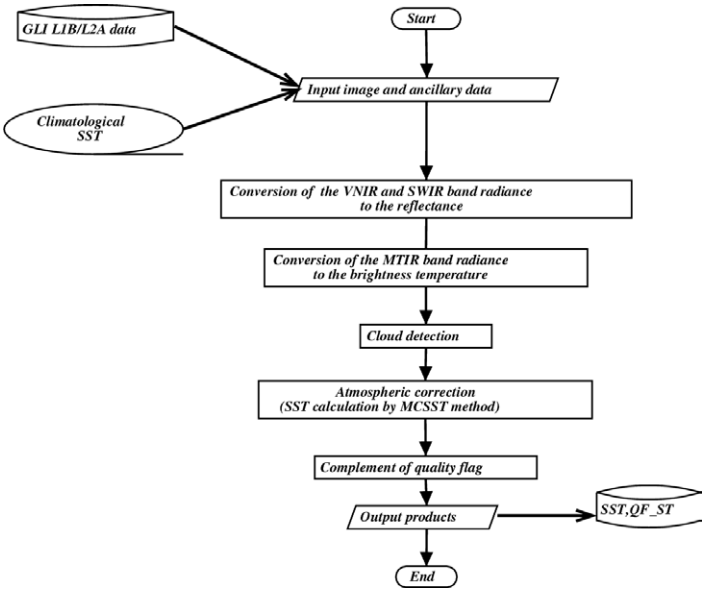

Figure 1. The flow chart of the whole process.

As shown in Figure 1, the SST data (SST) and the quality flag data (QF_ST) are produced using the GLI data and the climatological SST data. As for the GLI data, the following 10 bands are used: Band-8(0.545 μm), -13(0.678 μm), -19(0.865 μm), -26(1.24 μm), -27(1.38 μm), -30(3.7 μm), -31(6.7 μm), -34(8.6 μm), -35(10.8 μm), and -36(12 μm). The radiances are converted to reflectance, R, for visible and near infrared band (band 8-27), brightness temperature, BT, for thermal infrared band (band 30-35). CLFLG_p (Ackerman's cloud mask data) is also needed. As for ancillary data, the climatological SST data are needed for the quality control (QC). The specification of QF_ST is shown in the following table (Table 1). QF_ST is partly filled in the cloud detection process and the atmospheric

correction process and is complemented after these processes.

Table 1. The specification of the GLI SST flag data.

BIT FIELD	DESCRIPTION KEY	RESULT
1	Land/Sea	0=Sea / 1=Land
2	Cloud	0=Clear / 1=Cloudy
3	Lack of observation	0=No / 1=Yes
4	Large emmision angle1)	0=No / 1=Yes
5	Out of valid range2)	0=No / 1=Yes
6	Day/Night	0=Day / 1=Night
7	Sun glint	0=No / 1=Yes
8	Forward tilt	0=No / 1=Yes
9	Backward tilt	0=No / 1=Yes
10-11	Ackermann's four cloud class	00=cloudy 01=probably cloud 10=confident clear 11=high confidence clear
12-16	Spare	

1)The threshold of scan angle is 55 degree.

2)The threshold of the difference between GLI SST and climate SST is TBD.

Cloud detection: The framework of cloud detection algorithm is to apply up to some threshold tests and then to identify a pixel as cloud-free when all tests prove negative. Figure 2 shows processing flow of the cloud detection. We use ``scheme'' to represent the combination of cloud detection tests. Scheme-3 (nighttime) cloud detection algorithms are used when the solar zenith angle is greater than θ_{a0}<86.5 degree.

In the daytime, scheme-1 algorithms apply to the exterior of the sunglitter; scheme-2 are used to sunglitter region. To specify the sunglitter region, the reflection angle, θ_r, is used. θ_r is calculated by,

$$\cos\theta_r = \frac{\cos\theta_{suz} + \cos\theta_{saz}}{2\cos\omega}, \tag{1}$$

where ϕ_{saz} is satellite zenith angle. ω can be derived by,

$$\cos 2\omega = \cos\theta_{saz}\cos\theta_{suz} - \sin\theta_{suz}\theta_{saz}\cos(\phi_{sua} - \phi_{saa}), \tag{2}$$

where ϕ_{sua} and ϕ_{saa} are the azimuthal angles of the sun and the satellite, respectively. This geometry is shown in Figure 3. The limit value θ_{r0} for specifying sunglitter region is 30 degree. It is determined empirically as will be explained later.

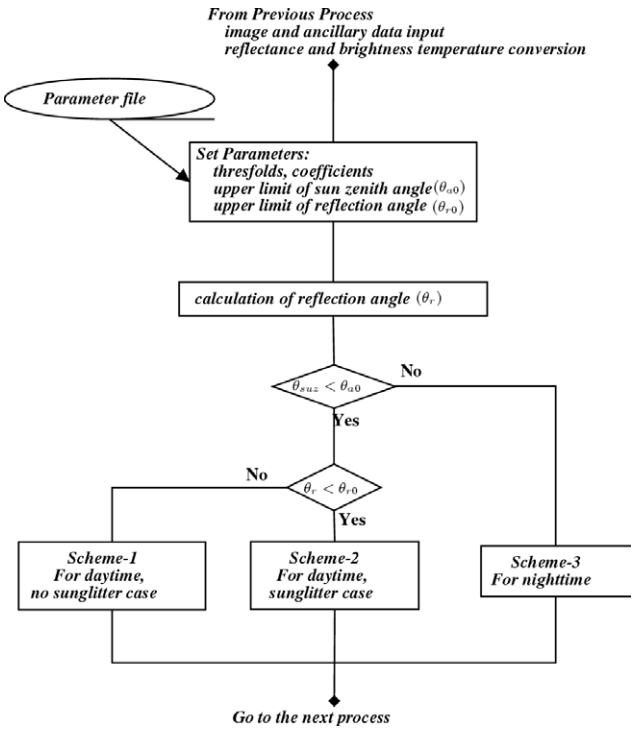

Figure 2: The processing flow of the cloud detection.

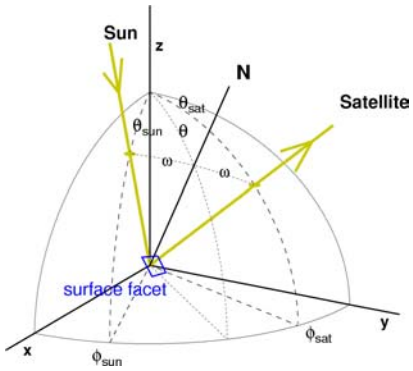

Figure 3: The reflection geometry between the sun, the satellite, and the surface facet

Table 2: Cloud detection tests for GLI-SST. The tests checked by ◎ are used in each scheme. Scheme-1: Daytime, outside the sun glint region. Scheme-2: Daytime, in the sun glint region. Scheme-3: Nighttime. BT_α :Brightness temperatures at α μm, $R\alpha$:reflectance at α μm, φ : latitude, : θ_r reflection angle,∇_{mn}: Max-Min difference in 3x3 box,∇_{mv}: Max-Center pixel value difference in 3x3 box. Overline on $BT_{10.8}$-BT_{12} denotes the mean in 3x3 box except for maximum value. FR: Full Resolution product, LR: Low Resolution product.

Group	Cloud detection test	Scheme		
		1	2	3
Gross test	$BT_{10.8}$<-0.007φ^2+283	○	○	○
	$BT_{10.8}$<269.15	○	○	○
Reflectance test	$R_{0.865}/R_{0.545}$ > 1.05-0.019 θ_r	×	○	×

	$R_{0.865}/R_{0.545} > 0.48$	○	×	×
	$R_{0.865} > 30.0\text{-}0.50\theta_r$	×	○	×
	$R_{0.865} > 15.0$	○	×	×
	$R_{1.38}>0.2$and $R_{0.865}/R_{0.545} > 0.4$	○	○	×
BTD test	$BT_{8.6}\text{-}BT_{10.8} > -0.5$	○	○	○
	$BT_{10.8} - BT_{12} > \exp(0.176BT_{10.8}\text{-}50.5) +1.45$	○	○	○
	$BT_{10.8} - BT_{12} > 4.3$	○	○	○
	$1.5\ BT_{3.7}\text{-}2.5\ BT_{10.8}+BT_{12} >3.5$	×	×	○
	$1.5\ BT_{3.7}\text{-}2.5\ BT_{10.8}+BT_{12} <-2.5$	×	×	○
	$0.6BT_{3.7}\text{-}0.6BT8.6 + BT_{10.8}\text{-}BT_{12} <1.8$	×	×	○
	$BT_{3.7}\text{-}\ BT_{12} <\ \exp(0.0345BT_{10.8}\text{-}9.375) + 1.$	×	×	○
Uniformity test	$\nabla_{mv}\ BT_{10.8}>1.5\ \nabla_{mn}(BT_{10.8} - BT_{12})> 2.5$	○	○	○
	$\nabla_{mn}\ R_{1.24} > 2.5$	○	○	×
	$\nabla_{mn}\ BT_{3.7} > 1.25$(FR) 2.0 (LR)	×	×	○

The first group is called as a gross cloud test. A pixel is flagged as cloudy when the brightness temperature of band-35 (10.8 μ m) is lower than the thresfold value. Tanahashi et al. (2000) used quadratic function of latitude as the thresfold value for S-VISSR/GMS. We adopted their forms with coefficients derived from GLI data empirically. Constant thresfold is used in conjection with quadratic function to identify clouds in high latitude regions.

The second tests use visible and near-infrared reflectance (R). These tests are widely used for retrieving SST from visible and infrared radiometer (e.g., Sakaida et al., 2000; Ackerman et al., 1997; Saunders and Kriebel, 1988). Reflectance ratio tests utilize the difference in reflection from cloud versus earth surface in wavelength above and below 0.72 μ m (Ackerman et al., 1997). Early studies used the 0.87 μ m reflectance divided by 0.66 μ m reflectance ($R_{0.865}/R_{0.545}$). Based on GLI data, it is found that $R_{0.865}/R_{0.545}$ (band-19 reflectance divided by band-8 reflectance of GLI) is more efficient for classifying cloud and ocean than $R_{0.865}/R_{0.678}$ (band-19 reflectance divided by band-13 reflectance). Figure 4 shows the scatter diagrams of $R_{0.865}/R_{0.545}$and $R_{0.865}/R_{0.678}$ from GLI data. It reveals that the former can distinguish the clear ocean from cloudy even in the sunglitter region. In order to avoid the potential for masking clear pixels in sunglitter region, the linear theresfold function and sunglitter region (θ r<30 degree) are defined empirically. Reflectance test for band-19 ($R_{0.865}$) is used additinally and the thresfold is determined as a function of reflection angle empirically.

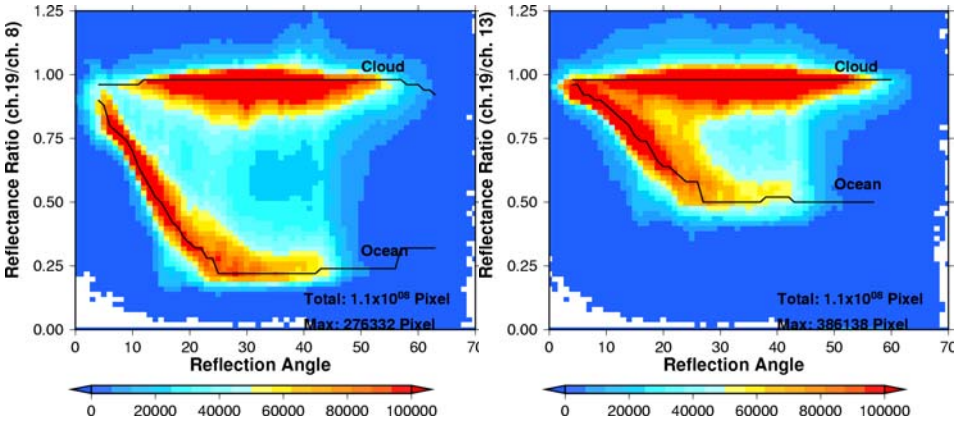

Figure 4: Scatter diagram of reflectance ratio and reflection angle based on GLI data. (Left) $R_{0.865}/R_{0.545}$ (band-19 reflectance divided by band-8 reflectance), (Right) $R_{0.865}/R_{0.678}$ (band-19 reflectance divided by band-13 reflectance). Color shows the frequency of appearance.

The third tests are brightness temperature difference (BTD) tests. The test using BTD between 11 μ m(band-35:10.8 μ m) and 12 μ m (band-36) is widely known as split window method, which is useful for detecting relatively thin clouds. It is known that the BTD depends on the brightness temperature of 11 μ m ($BT_{10.8}$). Saunders and Kriebel (1988) defined the thresfold as a function of satellite zenith angle and $BT_{10.8}$for AVHRR/NOAA. Stowe et al. (1999) suggested the 5-th order function of $BT_{10.8}$as the thresfold for cloud classfication from AVHRR/NOAA. Based on these reserches and the GLI data, the thresfold function for GLI is determined as exponential function of $BT_{10.8}$ (band-35) empirically. In addition, to avoid the striping noise and masking the frontal region, BTD is averaged over 3x3 pixel box except for maximum value. The test using BTD betwenn 8.6 μ m (band-34) and 10.8 μ m (band-35) is also useful to detect cloud. It is known that this BTD indicates ice cloud (Strabara et al., 1994). Since the dependency on the $BT_{10.8}$is weak, the thresfold of this test is determined as constant value. For nighttime observation, BTDs between 3.7 μ m (band-30) and other bands are used as cloud detection tests. Stowe et al. (1999) used BTD between 3.7 μ m and 12 μ m with a thresfold function of $BT_{10.8}$for nighttime test. Sakaida et al. (2000) and Guan et al. (2003) used the combination of $BT_{3.7,}$ $BT_{10.8}$and $BT_{12}$to detect cloud in nighttime. The combination of $BT_{3.7,}$ $BT_{8.6.}$ $BT_{10.8}$and $BT_{12}$is useful for detectinl low-level cloud in high latitude regions. The coefficients of these tests are adjusted to GLI data.

The forth tests are uniformity tests, which is based on the fact that brightness temperatures and reflectances on clear ocean are spatially homogeneous compared with cloudy regions. While these tests are very powerful, its reliability is low in the coastal and frontal regions. Since the tendency for cloudy condition is colder than clear condition, uniformity of $BT_{10.8}$ (band-35) is confirmed by the BTD between maximun in 3x3 pixel box and the center pixel value, which is used in Rossow and Garder (1993). In addition, the uniformity of BTD ($BT_{10.8-}$ BT_{12}) is combined to avoid masking the frontal region as cloud. The uniformity of BTD and reflectance are calculated by maximum and minumum difference in 3x3 pixel box. For nighttime, uniformity of $BT_{3.7}$ (band-30) is used. Thresfold for $BT_{3.7}$ uniformity test is changed as FR (full-resolution) and LR (low-resolution), since noise at GLI band-30 is so large that the spatial homogeneity of $BT_{3.7}$ in clear region of LR is less than that in FR. These thresfolds are determined empirically.

Atmospheric correction:In the GLI SST product, the MCSST method is used to retrieve the SST in clear pixels. The MCSST equation is the same form as one used in OCTS/ADEOSS SST algorithm (Sakaida et al., 1998) as follows:

$$\mathrm{SST} = a_0 + a_1 BT_{11} + \sum_{\lambda=3.7,8.7,12} \alpha_\lambda \overline{BT_{11} - BT_\lambda} + \sum_{\lambda=3.7,8.7,12} \beta_\lambda \overline{BT_{11} - BT_\lambda}(\sec\theta_{saz} - 1) \quad (3)$$

where θ_{saz} is a satellite zenith angle, α_λ and β_λ are the coefficients for BTD between 11 μm and λ μm. BTD between 11 μm and 3.7 μm is used in nighttime

The GLI MCSST equation contains $BT_{8.6}$, which is not observed by well-known split-window bands. The reason is that the use of this band is possibly advanced in the accuracy of SST estimation according to the study of OCTS and the numerical simulation (Moriyama et al., 1999).

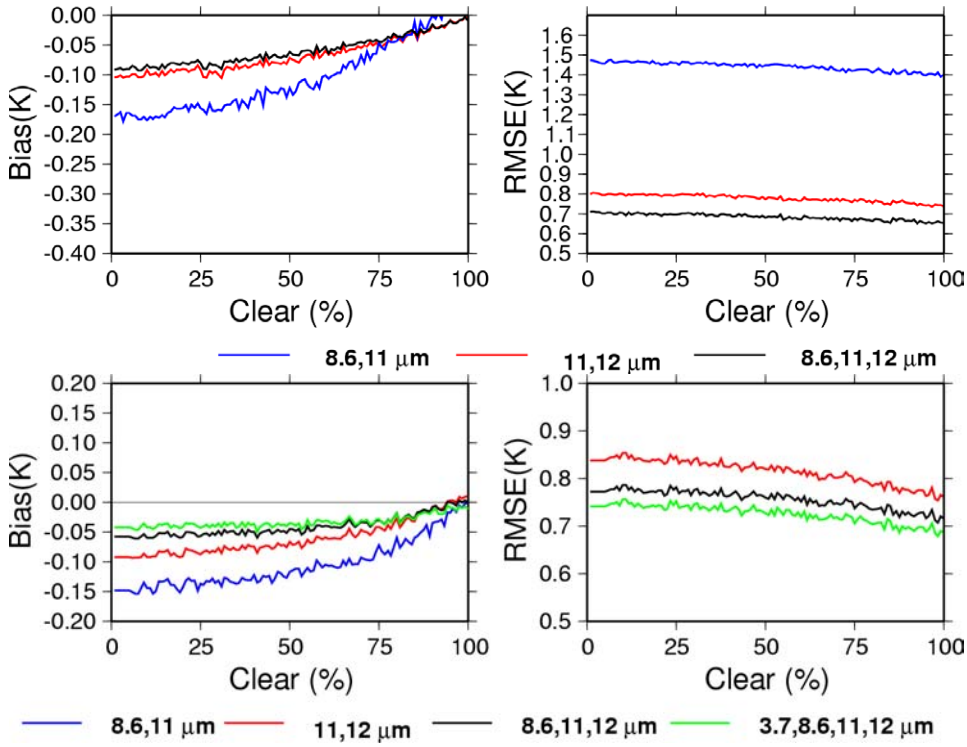

Figure 6: Relation of bias and RMSE between the MCSST algorithms and the clear rate around the buoy points, for daytime (top) and nighttime (bottom). The matchup points are shown in Figure 9. Each line denotes the MCSST algorithm using brightness temperature differences between the bands shown below the figures.

The effect of including $BT_{3.7}$ and $BT_{8.6}$ in MCSST equation can be denoted from the comparison between the GLI-estimated and buoy-measured SST (observation points shown in Figure 9). Figure 6 shows the bias and RMSE of several MCSST algorithms as a function of clear rate, which is defined as the ratio of number of clear pixels and whole pixels (11x11 array) around the buoy point. In the daytime, triple-window algorithm using 8.6, 11 and 12 μm is able to obtain the better estimation of bulk SST than the split window algorithm. In the nighttime, the estimated SST data from the algorithm including 3.7 μm are accurate even if the clear rate is low (near cloud region).

To reduce the noise effects, brightness temperature difference terms are averaged for NxN pixel array. The following chart (Fig. 7) shows the SST calculation process with the detail of this averaging. Using GOES data, Wu et al. (1999)

pointed out that the optimal box size of averaging brightness temperature differences is as small as 3x3 array for representative of a buoy measurement, since the RMSE (root-mean-square-error) of satellite-estimated and buoy-measured SSTs is minimum using 3x3 array averaging. From GLI data, the minimum valud of bias between GLI-estimated and buoy-measured SST (observation points are shown in Figure 9) is denoted when the averaging size is 7x7 array, while RMSE monotonically decreases with array size (Fig.5). Since RMSE difference of 7x7 array and 9x9 array is small, it is suggested that 7x7 array is optimal for GLI SST. Figure 7 shows the chart of SST calculation process.

The coefficients of Eq.(3) are derived by the pre-launch numerical simulation (see Appendix). After the launch of the ADEOS-II, the match-up data are collected. Using the match-up data, the coefficients of Eq.(3) are also derived. For the development of version 1.0 algorithm, the match-up data in 3/19-22 and 4/2-7 are used. The number of the match-up data is 546. In the pre-launch and version 1.0 algorithm, the BTD between 3.7 μ m and 11 μ m is not used and the same MCSST euqation is used for daytime and nighttime. In version 2.0 algorithm, the different coefficients are used for daytime and nighttime separately. The match-up data in 4/2-7/31 are used. The numbers of total match-up data are 5880 (daytime) and 5327 (nighttime), respectively. The time difference between the satellite and in-situ observation is within 2 hours and the clear-rate around the in-situ observation point is more than 95%. The one-fifth of the total data are used to derive the coefficients, while the unused data are applied to the validation (Section 3). The coefficients are shown in Table 3.

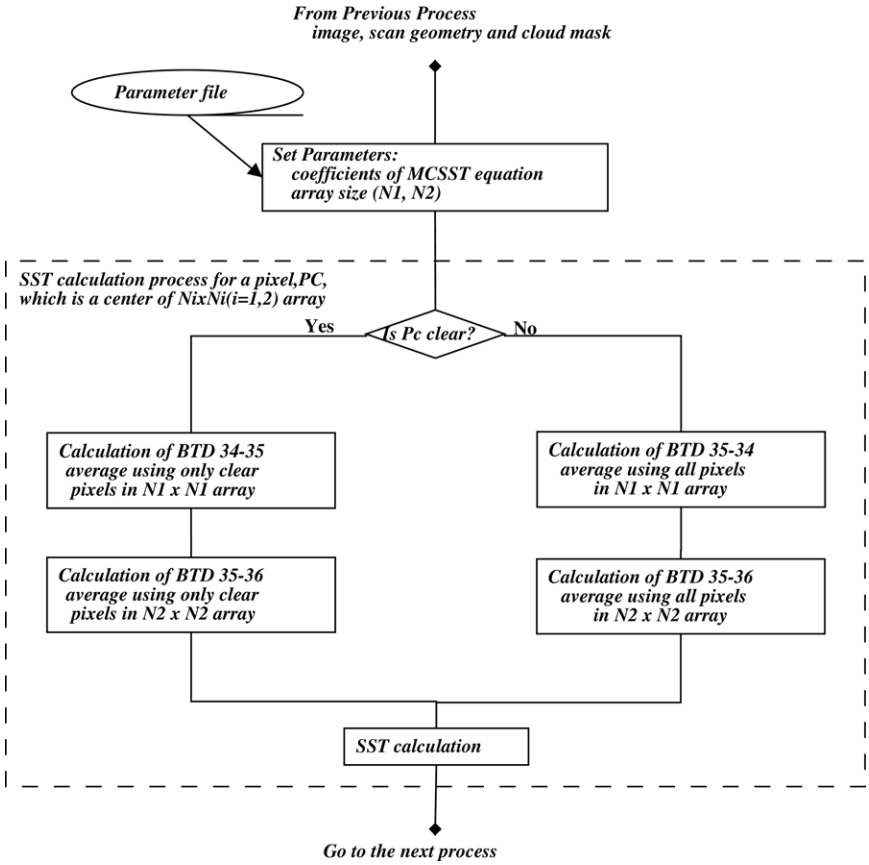

Figure 7: The SST calculation process with the detail of this averaging.

Table 3: The coefficients used in MCSST equation (3). Num and Period means the number and collected period of match-up data, respectively.

Satellite	Day/Night	Num	Period	a_0	a_1	
Pre-launch	Day and Night	(Sim)	(Sim)	2.276	0.9966	
Version 1.0	Day and Night	546	3/19-22, 4/2-7	-2.35069	1.019241	
Version 2.0	Day	1006	4/2-7/31	2.104985	1.004573	
	Night	1105	4/2-7/31	7.896403	1 0.9775310	

	$\alpha_{3.7}$	$\alpha_{8.6}$	α_{12}	$\beta_{3.7}$	$\beta_{8.6}$	β_{12}
	0.0	-0.2106	1.946	0.0	0.2481	0.507
	0.0	-1.11811	1.863587	0.0	0.272058	1.020815
	0.0	-1.535977	1.954971	0.0	0.4978902	0.8223422
	-0.8817639	-0.5275608	1.146796	-0.2944342	0.1940683	0.2518997

Quality Control: I The quality control (QC) process is included in OTSK13, for decreasing the cloud contaminated pixels after the cloud detection. In OTSK13, the quality control is defined as the checking process of SST value compared with reference SST after the cloud detection and SST caluculation process.

The QC process consists of the following two processes. At first, SST value $SST_{GLI}(x,y)$ derived by GLI at a fixed point is compared with the SST dataset $SSTT_{clim}$ by Reynolds and Smith (1994), which is monthly climatological data with spatial resolution of0.25x0.25 degree. Given the standard deviation of SST ⊿ SST_{clim}, the pixel is flagged if the following equation is satisfied.

$$|SST_{GLI} - SST_{clim}| > 2⊿\ SST_{clim}. \quad (4)$$

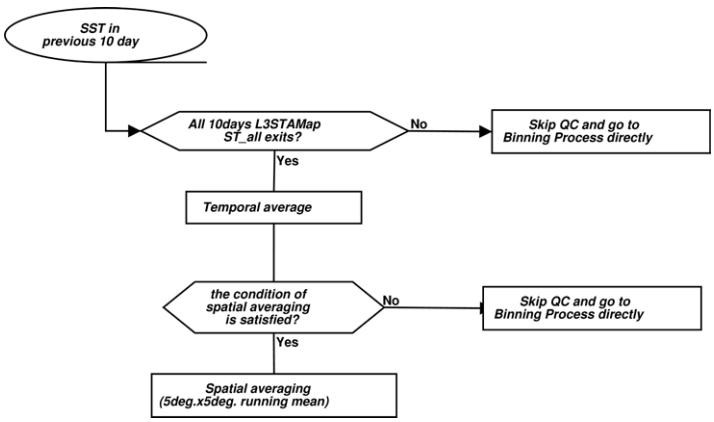

Figure 8: The flowchart of the past 10 days L3STAMAP data for QC

The second QC process is used to masks the suspectable data in the Level 3 products. Past 10 days Level 3 daliy-mean SST product (L3STAMAP) is used as an ancillary data. The past 10 days data are smoothed by spatial running average over 5x5 degree . If the center pixel is lacked in past 10 days product or the number of valid pixels located in spatial averaging area is less than 10%, the QC process at the pixel is skipped. After the ancillary data are obtained, the SST value at a fixed point is flagged if the difference between the value and ancillary data at the point is larger than an acceptable differences of SST. The acceptable difference is defined as constant values(6K in daytime, 4K in nighttime).

Validation: For validating the SST product from OTSK13, mutchup data of GLI-estimated SST and buoy-measured SST are used. Buoy observation is quality checked using climatological SST. The mutchup is collected from 174 days (from Apr. 02 to Oct. 24), if time difference between buoy and GLI observations is less than 3 hours. The match-up data used to derive the coefficients in MCSST equations are not used in the validation. Through the quality control in which more than 110 pixels in 11x11 pixel array around the point are clear, the numbers of match-up are 7108 (daytime) and 8767 (nighttime), respectively.

Figure 9 shows the mutchup measurements points and scatter diagram of GLI and buoy SST. The biases and RMSEs of the difference between GLI and buoy SST are 0.03K and 0.66K for daytime, -0.01K and 0.70K for nighttime, respectively.

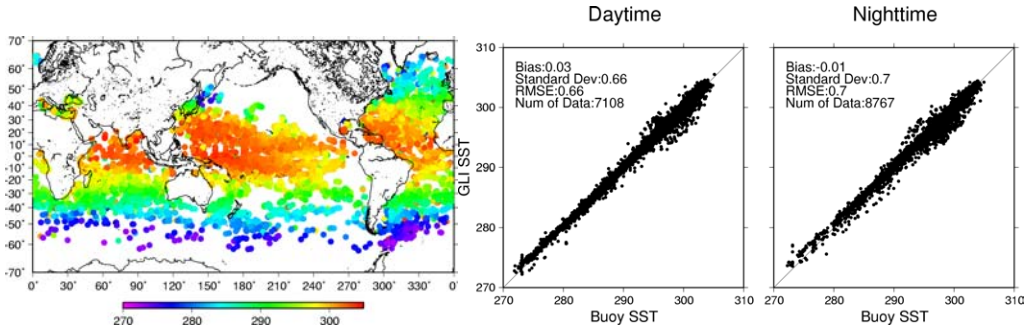

Figure 9: (Left)Location of the mutchups. Color denotes the buoy measurement SST. (Right) Comparison of GLI estimated SST and buoy measurements.

Figure 10 shows the timeseries of statistics between the GLI and buoy SST. The biases in early phase are positive, while they in latter phase are low or negative. RMSEs have a peak in August. In all period, bias and RMSE are less than 0.10 and 1.0 K, respectively.

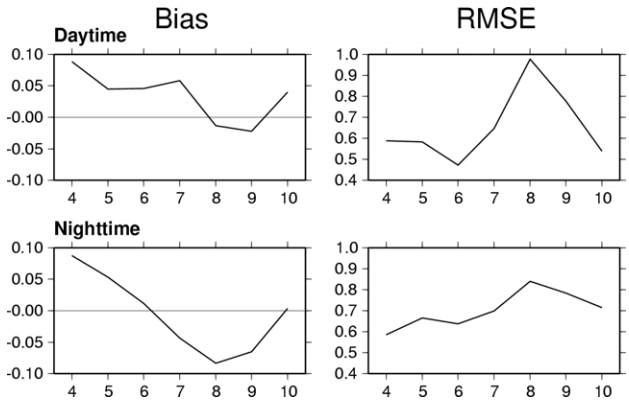

Figure 10: Time-series of biases and RMSEs between the GLI MCSST and buoy bulk-SST.

C. Practical Considerations

(1) Programming, Procedural, Running Considerations

Program Requirements: The following table shows information about the expected software generated from this algorithm

Program Memory	
Program Size	
Required Channels	Band-8, -13, -19, -26, -27, -30, -31, -34, -35, and -36.
Necessary/Ancillary Data	CLFLG_p (Ackerman's cloud mask data), the climate SST data, and the parameter file.
Expected Disk Volume	
Special Programs or Subroutines	See the document on the program example for GLI synthetic data.

(2) Calibration and validation

Cloud detection algorithm:

To adjust the cloud detection tests, GLI L1B and L2A data is needed.

Atmospheric correction algorithm:

Match-up data set is needed to derive the coeffcients of the MCSST equations.

(3) Quality Control and Diagnostic Information

(4) Exception Handling

(5) Constraints, Limitations, Assumptions– See cited literature

(6) Publications and Papers

D. References

Ackerman, S. A., K. Strabala, W. P. Menzel, R. A. Frey, C. C. Moeller, L. E. Gumley, B. A. Baum, C. Shaaf, and G. Riggs, 1997: Discriminating clear sky from cloud with MODIS algorithm theoretical basis ducument (MOD35). Eos ATBD web site,125pp.

Guan, L., H. Kawamura, and H. Murakami, 2003: Retrieval of sea surface temperature from TRMM VIRS. J. Oceanogr., 59, 245-249.

Moriyama, M., F. Sakaida, and H. Kawamura, 1999: Characteristics of 8μ m band in terms of the global sea surface temperature retrieval, (in preparation).

Reynolds, R. W. and T. M. Smith, 1994: Improved global sea surface temperature analysis using optimum interpolation. J. Clim., 7, 929-949.

Rossow, W. B. and L. C. Garder, 1993: Cloud detection using satelite measurements of infrared and visible radiance for ISCCP. J. Clim., 6, 2341-2369.

Sakaida, F., J.-I. Kudoh, and H. Kawamura, 2000: A-HIGHERS-The system to produce the high spatial resolution sea surface temperature maps of the western North Pacific using the AVHRR/NOAA. J. Oceanogr., 56, 707-716.

Sakaida, F., M. Moriyama, H. Murakami, H. Oaku, Y. Mitomi, A. Mukaida, and H. Kawamura, 1998: The sea surface temperature product algorithm of the Ocean Color and Temperature Scanner (OCTS) and its accuracy. J. Oceanogr., 54, 437-

442.

Saunders, R. W. and K. T. Kriebel, 1988: An improved method for detectiong clear sky and cloudy radiance from AVHRR data. Int. J. Remote Sensing, 9, 123-150.

Stowe, L. L., P. Davis, and E. P. McClain, 1999: Scientific basis and initial evaluation of the CLAVR-1 global clear/cloud classification algorithm for the Advanced Very High Resolution Radoimeter. J. Atmos. Oceanic Technol., 16, 656-681.

Strabara, K. I., S. A. Ackerman, and W. P. Menzel, 1994: Cloud properties inferred from 8-12-μ m data. J. App. Meteor., 33, 212-229.

Tanahashi, S., H. Kawamura, T. Matsuura, T. Takahashi, and H. Yusa, 2000: Improved estimate of wide-ranging sea surface temperature from GMS S-VISSR data. J. Oceanogr., 56, 345-358.

Wu, X., W. P. Menzel, and G. S. Wade, 1999: Estimation of sea surface temperarures using GOES-8/9 radiance measurements. Bull. Amer. Meteor. Soc., 80, 1127-1137.

Appendix Physical and Mathematical aspects of the algorithm

Atmospheric correction The coefficients of the split-windows equation will be defined from the multivariative regression using the match-up dataset which has the satellite detected brightness temperature and the scan geometry collocated with the sea surface temperature which are measured by buoys, ships, aircrafts and so on. For the initial definition of the split-window formula, it is desireable to define the function type which can make the stable estimation under the real observation.

For the Global mapping, the error of the estimated SST must be independent from the observed brightness temperature. The following is the mathematical expression of this concept,

$$\delta t = \Sigma (df/dTi)\, \delta Ti \qquad (1)$$

where δt, f and δTi are the error of the estimated SST, the split-window function and the observation error of the brightness temperature of ith spectral channel respectively. The partial derivative of the split-window function is constant when the split-window function is linear, so that the estimation error of the SST will be independent from the brightness temperature. From this reason, the GLI split-window function is defined as the linear function.

For the function type definition, the numerical simulation, which is based on the model atmosphere/surface conditions, is described as follows.

Model atmosphere: 1990 Monthly mean NCEP dataset, Longditudal averaged over 10 [deg.] latitude interval (12 x 18 = 216)
Other gas amount: NRL model
Model SST: T(0) + 1 [K] + normal random variable with 5/3 [K] standard deviation.
observation zenith: 0, 30, 60 [deg.]
Radiative transfer code: MODTRAN 3.5
Computation item: brightness temperature at GLI 34, 35, 36channels.
Observation error: Normal random variable with 0, 0.1, 0.2 [K] standard deviation.
Aerosol type: Rural

Aerosol amount: Surface visibility: 23 [km] (@550nm)
Model emissivity: 1.0, 0.99, 0.98, 0.97

From these conditions, the brightness temperature at GLI channels 34, 35 and 36 are computed. By using the above dataset, the multivariative regression analysis based in the following formulae are made.

SST = a T35 + b (T35-T36) + f (2)

SST = a T35 + b (T35-T36) + c (T35-T34) + f (3)

SST = a T35 + b (T35-T36) + c (T35-T34) + d (T35-T36)(1/cos □s-1) + f (4)

SST = a T35 + b (T35-T36) + c (T35-T34) + d (T35-T36)(1/cos □s-1) + e (T35-T34)(1/cos □s-1)+ f (5)

The RMS error of the estimated SST under the no observation error case from the above formulae are listed below

Eq. RSME [K]

(2) 0.559

(3) 0.312

(4) 0.424

(5) 0.291

The Equation (5) show the most accurate result, so that this function type (5 terms formula) is used for the GLI split-window formula.

As the preliminary set of the coefficients are defined from the following scheme.

1.The coefficient sets are defined from the common observation error and the surface emissivity.

2.Compute the RMS error of the estimated SST from the all brightness temperature data based on each coefficient set.

3.The coefficient set which minimize the RMS error is selected as the preliminary set.

Bias and RMS error from the each coefficient set are listed below.

ε NEdT RMS [K]

0.97 0.0: 0.634702

0.97 0.1: 1.0413

0.97 0.2: 1.34708

0.98 0.0: 0.56707

0.98 0.1: 0.816566

0.98 0.2: 0.969785

0.99 0.0: 0.582015

0.99 0.1: 0.743614

0.99 0.2: 1.20846

1.00 0.0: 0.659112

1.00 0.1: 1.0384

1.00 0.2: 1.25814

From the RMS error, the coefficient set for the condition, in which the surface emissivity is 0.98 and the observation noise is 0, are selected.

The preliminary coefficient set is as follows.

a = 0.9966, b = 1.946 , c = 0.2106, d = 0.5070, e = 0.2481, f = 2.276